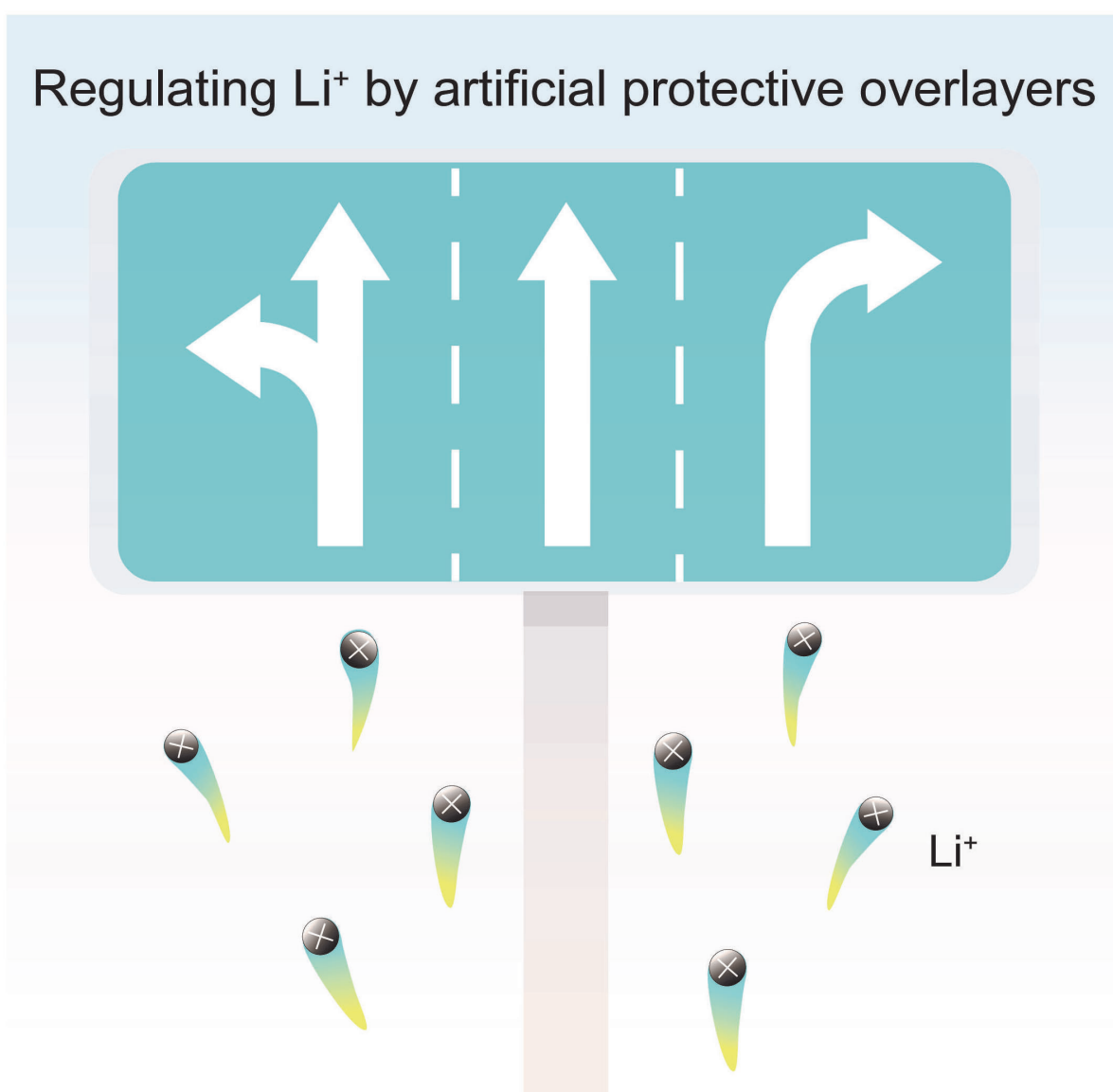


Regulating Interfacial Lithium Ion by Artificial Protective Overlayers for High-Performance Lithium Metal Anodes

Lei Ye,^[a] Meng Liao,^[a] Bingjie Wang,^{*[a]} and Huisheng Peng^{*[a]}



Abstract: The main limitation of lithium (Li) metal anodes lies in their severe dendrite growth due to nonuniform Li^+ flux and sluggish Li^+ transportation at the anode surface. Fabricating artificial protective overlayer with tunable surficial properties on Li metal is a precise and effective strategy to relieve this problem. In this Concept article, we focus on the

basic principles of regulating interfacial Li^+ through artificial protective overlayers and summarize the material preparation as well as structural design of these overlayers. The remaining challenges and promising directions of artificial protective overlayers are then highlighted to provide clues for the practical application of Li metal anodes.

1. Introduction

With the surging demand for high-energy and high-power batteries for electric vehicles and smart grids, lithium (Li) metal anode with a high specific capacity (3861 mAh/g) and a low potential (-3.04 V vs. standard hydrogen electrode) is deemed promising to afford higher energy beyond Li-ion batteries.^[1–3] Thus far, the practical implementation of Li metal anodes still calls for explorations since it is hindered by the growth of Li dendrites with the resulting deteriorated battery performances and related safety hazards.^[4–6] As is known, the formation of Li dendrites mainly originates from the non-uniform Li^+ distribution at the Li metal surface due to the heterogeneous solid-electrolyte interphase and Li^+ depletion induced space charge.^[7,8] Therefore, realizing uniform Li^+ flux at the Li metal surface can solve the above problems at their source for a dendrite-free Li metal anode. To achieve this goal, numerous strategies have been proposed, mainly including three-dimensional (3D) nanostructured hosts,^[9–12] electrolyte engineering,^[13–15] and artificial protective overlayers.^[16–18]

Among various strategies, incorporating artificial protective overlayers on Li metal becomes increasingly popular for dendrite-free Li metal anodes. On one hand, artificial protective overlayers can be accurately designed to achieve desirable surficial properties (e.g., homogeneous chemical component and high mechanical strength) for uniform Li^+ distribution at electrode surface.^[19,20] On the other hand, the regulation and acceleration effect of interfacial Li^+ transportation from artificial protective overlayers contributes to a relieved Li^+ depletion with less distorted space charge at the electrode surface during Li^+ deposition.^[21–23]

In this Concept article, we will briefly discuss the recent advances in artificial protective overlayers composed of inorganic salts, organic polymers, and carbonaceous materials for interfacial Li^+ regulation, with emphasis on material designs and working mechanisms. The remaining challenges and potential directions for artificial protective overlayers are then

highlighted to enlighten their future implementation for stable Li metal anodes.


2. Inorganic Li^+ Conductive Protective Overlayers

Inorganic protective overlayers are known for their high mechanical strength to physically block dendrite penetration.^[23,24] In contrast, despite its feasibility, using inorganic overlayers to regulate Li^+ conducting behaviour aroused much fewer attention.^[25] Leveraging the constitution of inorganic overlayers to direct the Li^+ flux along desired pathways can afford uniform Li^+ distribution on electrode surface with less aggregation.^[8,26] In this regard, several protective overlayers composed of inorganic salts (e.g., Li_3N , LiF and Li-rich alloy) have been fabricated to regulate and homogenize Li^+ flux for dendrite-free Li anodes.^[27,33,39]

2.1. Li_3N

Li_3N is a promising component for artificial protective overlayer due to its low electrical conductivity ($< 10^{-12}\text{ S/cm}$), high ionic conductivity (up to 10^{-3} S/cm), and high Young's modulus (up to 48 GPa).^[27,28] Its lamellar crystal structure allows rapid Li^+ motion along layers and benefits its high ionic conductivity (Figure 1a–c).^[29] Moreover, negative charges on the nitride ions form a space charge layer at the surface, enhancing surficial Li^+ diffusion and promoting smooth Li depositing. The Li_3N protective overlayer could be fabricated through ex situ methods, such as mechanically compressing Li_3N particles into thin films stacked on Li metal and drop coating the Li_3N /binder mixture to form Li_3N droplets on Li metal.^[30,31] However, these ex situ formed Li_3N overlayers exhibited unsatisfying ionic conductivity due to their as-prepared, porous structures comprised of weakly interconnected and randomly dispersed crystal grains (Figure 1d). Controlling the nanostructure and crystal grain orientation can promote the ionic conductivity of Li_3N overlayers. To this end, an in situ fabrication method of reacting clean molten Li foil with pure nitrogen gas was reported to obtain a pinhole-free Li_3N overlayer with strongly interconnected, large crystal grains (Figure 1e).^[29] The pinhole-free Li_3N overlayer was vertically bonded to Li metal along the [001] lattice plane of Li_3N . The large grain size and oriented crystals of this compact Li_3N overlayer rendered a high ionic

[a] L. Ye, Dr. M. Liao, Dr. B. Wang, Prof. H. Peng
Laboratory of Advanced Materials
State Key Laboratory of Molecular Engineering of Polymers, and
Department of Macromolecular Science
Fudan University
Shanghai 200438 (P. R. China)
E-mail: wangbingjie@fudan.edu.cn
penghs@fudan.edu.cn

 Selected by the Editorial Office for our Showcase of outstanding Review-type articles <http://www.chemeurj.org/showcase>.

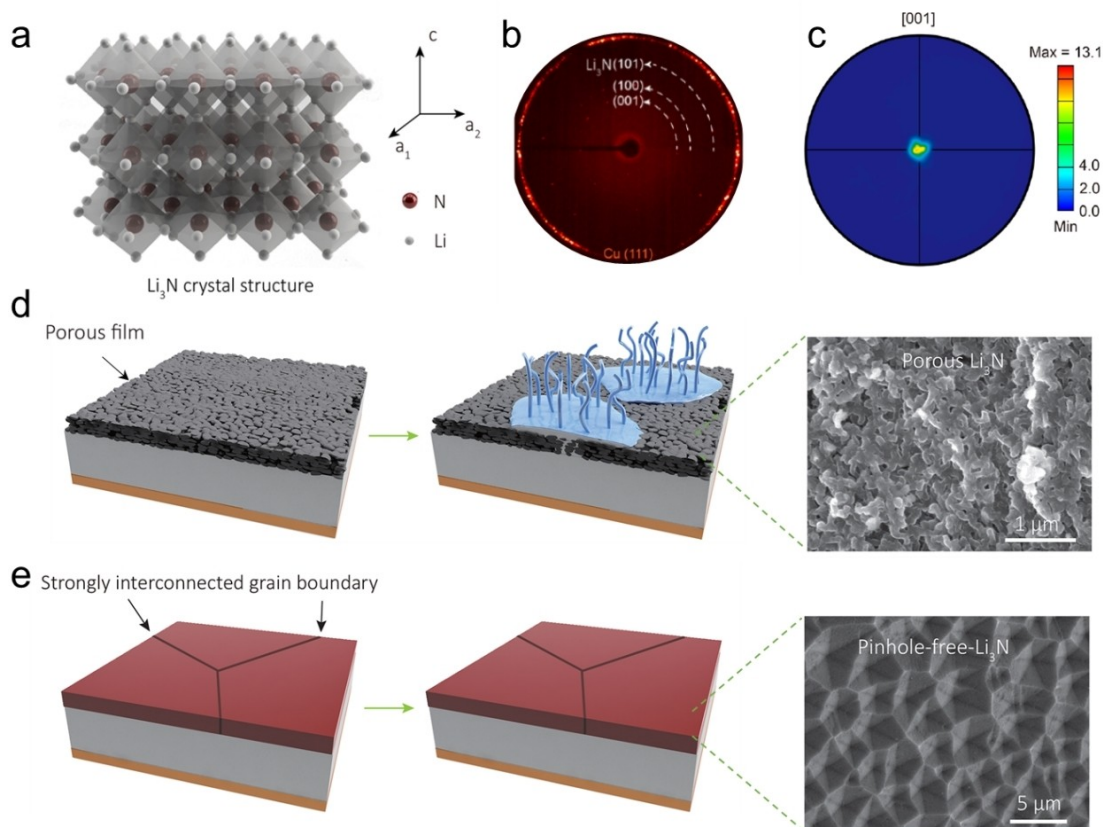


Figure 1. a) Schematic of Li_3N crystal structure. b) 2D X-ray diffraction pattern of the Li_3N crystal. c) Pole figure of the [001] plane of a compact Li_3N layer. d) A Li metal anode modified with a porous Li_3N overlayer. e) A Li metal anode modified with a dense Li_3N overlayer. Reproduced with permission.^[29] Copyright 2018, American Chemical Society.

conductivity of $5.2 \times 10^{-4} \text{ S/cm}$, supporting rapid Li^+ transfer and relieving Li^+ depletion. With a pinhole-free Li_3N overlayer, dendrite growth had been restrained and the $\text{Li}|\text{Li}_4\text{Ti}_5\text{O}_{12}$ cell had achieved a stable cycling performance over 500 cycles at 1 C. More recently, a flower-shaped Li_3N protective overlayer with [001] plane orientation was synthesized through a nitrogen plasma technique, i.e., the nitrogen plasma generated by high radio frequency reacted with fresh Li metal to form Li_3N overlayer in situ.^[32] The fabrication process was carried out under a mild condition of room temperature within several minutes, demonstrating a potential in large-scale manufacturing. The obtained Li metal anode exhibited a stable cycling performance of 500 h at 0.5 mA/cm^2 and 1 mAh/cm^2 . It should be noted that, despite of the above advantages, Li_3N has a narrow electrochemical stable window (0–0.44 V vs. Li), limiting its applications in high-voltage electrolytes.

2.2. LiF

LiF demonstrates many excellent properties, for example, a large bandgap (13.6 eV) and a wide electrochemical stability window (0–6.4 V vs. Li), making it a highly stable protective overlayer toward Li metal.^[33,34] According to the joint density functional theoretical studies, LiF exhibits a relatively low

energy barrier for surficial Li^+ diffusion and thus the Li^+ transport along the LiF surface is facilitated.^[35,36] This promoted surface conduction reduces the Li^+ aggregation at surficial defect and homogenizes Li^+ flux at the anode surface, inducing a lateral Li deposition without dendrite. In addition, the LiF-based overlayer with high surface energy is less vulnerable to the formation of fractures upon large volume change during Li plating/stripping. As a typical paradigm, an amorphous LiF overlayer was coated on a routine copper current collector by in situ hydrolysis of lithium hexafluorophosphate (LiPF_6) when copper foil was dropped into an aqueous LiPF_6 solution.^[37] The low Li^+ diffusion energy barrier along the LiF [100] surface afforded a rapid Li^+ diffusion, and the Li^+ adsorbed on the LiF surface could rapidly penetrate the LiF overlayer to deposit on copper substrate according to the DFT calculations (Figure 2a). The facilitated Li^+ transportation combining with chemical uniformity in the LiF overlayer concurrently enabled a uniform Li^+ distribution and an aligned columnar morphology of Li deposits (Figure 2b, c).

Optimizing and controlling the morphology and thickness of LiF overlayers could further improve the Li^+ flux compared with the amorphous ones. In this regard, a LiF overlayer was made by a physical method of radio-frequency magnetron sputtering deposition at room temperature.^[38] The thickness of LiF overlayer was rigorously controlled by the sputtering time

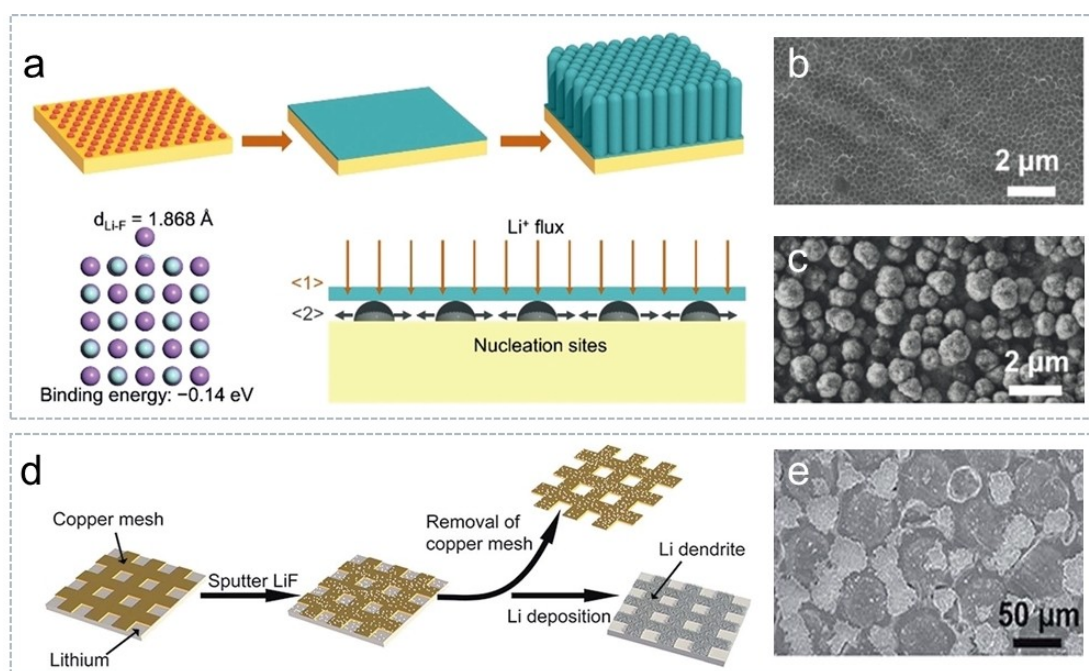


Figure 2. a) The binding energy of Li on the LiF [100] face and the schematic illustration for the Li deposition process with LiF protective overlayer. b) and c) The columnar morphology of Li deposits with LiF protective overlayer. Reproduced with permission.^[37] Copyright 2017, Wiley-VCH. d) Schematic demonstration of fabricating and Li deposition for the patterned LiF-coated Li metal anode. e) SEM image of the patterned LiF-coated Li anode after deposition. Reproduced with permission.^[38] Copyright 2017, Royal Society of Chemistry.

and the optimal thickness was determined as 150 nm. With this thickness, the Li^+ conduction was maximized with a restrained dendritic deposition. Further increasing the layer thickness increased the Li^+ transfer distance and interfacial resistance, resulting in the undesirable Li^+ depletion or Li^+ concentration polarization at the electrode surface. To directly evaluate the effect of LiF coating, patterned LiF overlayers with controllable holes were constructed on Li metal surface (Figure 2d). As expected, the area covered by LiF was smooth and compact in contrast to dendrite growth at hole sites without LiF protection (Figure 2e). It should be noted that LiF exhibited low Li^+ conductivities of $10^{-13} \sim 10^{-14} \text{ S/cm}$, which largely compromised its effectiveness in high-rate Li plating/stripping.^[27] Constructing hybrid LiF-rich protective overlayer with highly Li^+ conductive component, in this regard, presents a promising solution.

2.3. Li-rich alloys

Li-rich composite alloy (Li_xM , $\text{M}=\text{In, Zn, Bi, Al, and As}$) overlayer with much higher Li^+ diffusion coefficients ($10^{-8} \sim 10^{-6} \text{ cm}^2/\text{s}$) than that of Li metal ($5.69 \times 10^{-11} \text{ cm}^2/\text{s}$), can boost Li^+ penetration through the overlayer.^[39] More interestingly, pre-stored abundant Li^+ in the overlayer effectively relieves Li^+ depletion and Li^+ concentration polarization in the anode vicinity, leading to homogenized Li^+ flux. The Li-rich alloy overlayer is fabricated through a facile process of immersing Li metal in MCl_x solution. The thickness of alloy overlayer can be regulated by the immersion time and concentration of MCl_x

solution. The MCl_x is first reduced by Li metal: $x\text{Li} + \text{MCl}_x \rightarrow \text{M} + x\text{LiCl}$ ($\text{M}=\text{In, Zn, Bi, Al, and As}$) (Figure 3a).^[40] The generated metal then reacts with Li metal to produce a single phase composition: $y\text{Li} + z\text{M} \rightarrow \text{Li}_y\text{M}_z$. Although the alloy is a small band-gap semiconductor, the massive insulating LiCl co-product still renders the composite overlayer resistive. For instance, direct reduction of In_3Cl by Li metal at room temperature produced a highly ionic conductive overlayer (Li^+ conductivity at $2 \times 10^{-4} \text{ S/cm}$) composed of Li_3In_3 and LiCl.^[39] The protected Li metal anode exhibited a cycling life of 1400 h at a current density of 2 mA/cm^2 and the $\text{Li}|\text{Li}_4\text{Ti}_5\text{O}_{12}$ full battery cycled for 1500 cycles at a high rate of 5 C. Under the same guidance, a Li–Al alloy based protective overlayer was designed to obtain an ionic conductivity of $0.27 \times 10^{-4} \text{ S/cm}$ and an enhanced mechanical strength of 776 MPa.^[40] Benefited from the fast Li^+ transport and pre-stored Li^+ at the electrode surface, the resulting Li metal anode achieved an excellent rate performance at a high current density of 20 mA/cm^2 .

It should be noted that although the inorganic protective overlayers with high ionic conductivity contribute to rectify Li^+ flux and extend cycle life of Li anode, their intrinsic nature (e.g., fragility, rigidity, and non-flexibility) has restrained the application in high-areal-capacity cycling.^[41,42] In such circumstance, drastic volume change during Li plating/stripping may crack inorganic overlayers and lead to even exacerbated dendrite growth. Combining with elastic components to construct hybrid overlayers helps to promote the durability of inorganic overlayers, and the detailed discussion is presented in Section 3.3.

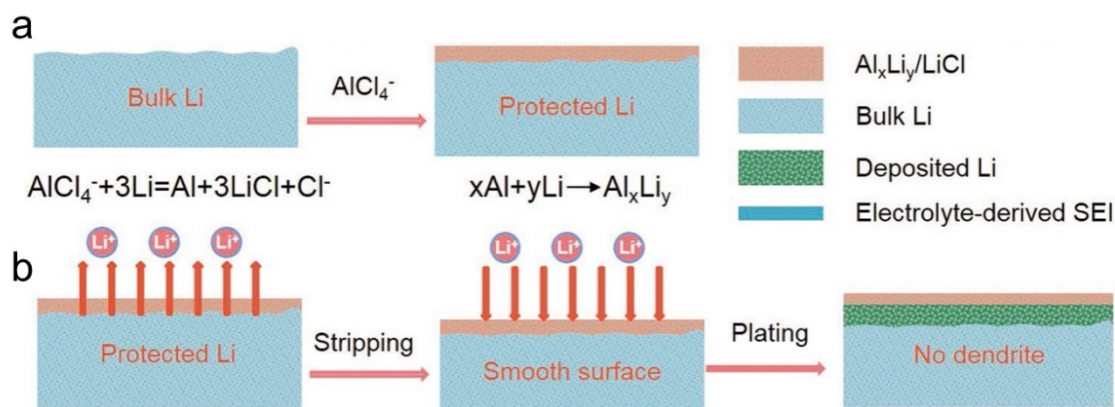


Figure 3. a) Schematic demonstration of the fabrication process of the Al_xLi_y alloy protective overlayer. b) The dendrite-free Li plating/stripping process with the Al_xLi_y alloy protective overlayer. Reproduced with permission.^[40] Copyright 2020, Wiley-VCH.

3. Polymeric Protective Overlayers

Polymeric protective overlayers, featured with high flexibility and tunable chemical diversity, are expected to endure large volume change and keep structural integrity during long-term and recurring Li plating/stripping.^[43–45] Designing polymeric overlayers with varying composition and structure can mediate the Li deposition for desirable performances. For instance, polymeric overlayers containing polar functional groups generally show strong interactions with Li^+ through chemical binding. This interaction enhances Li^+ extraction from the solvation sheath, changes the solvation structure, and affords relatively smooth Li deposition upon high current density due to the increased Li^+ diffusion rate.^[23] Besides, the Li^+ conducting properties can also be improved by synthesizing micro/nano-structured polymeric overlayers with optimized electrolyte pathways.^[45] Benefited from the structural and chemical tunability of polymeric overlayers, uniform Li^+ flux and fast Li^+ transportation at the interface can be achieved with a lateral Li deposition without dendrite.

3.1. Polar polymers

Lithiophilic polymeric overlayers with abundant polar functional groups, such as poly(ethylene oxide), polyacrylonitrile, polyimide, and polyurea, exhibit strong interactions between polar groups and Li^+ at molecular scale.^[47–49] It was demonstrated that an improvement in polarity of protective overlayer could render enhanced electrochemical performances of Li metal anodes.^[50] By tuning the crystal structure of polyvinylidene difluoride (PVDF), artificial protective overlayers based on polar β -phase PVDF (β -PVDF) and non-polar α -phase PVDF (α -PVDF) were fabricated.^[51] Compared with the α -PVDF/Li anode, the β -PVDF protected Li metal anode exhibited a lower voltage hysteresis, a higher coulombic efficiency, and a longer cycle life. These improved electrochemical performances clearly illustrated the importance of interaction between Li^+ and artificial protective overlayers. In addition, the alignment of F atoms in

the β -phase PVDF provided preferential diffusion pathways that helped Li^+ hopping across the overlayer to achieve high-rate Li deposition. Consequently, the β -PVDF/Li anodes realized a stable Li plating/stripping at a high current density of 5 mA/cm².

The interaction between protective overlayers and Li^+ could be further enhanced by the introduction of proton-containing polar functional groups, for example, $-\text{COOH}$, $-\text{NH}_2$, and $-\text{SH}$. Moreover, the interaction of Li with the polymer rendered a chelation between Li and electronegative atoms (e.g., N and O) among intra- and inter-polymer chains, leading to a crosslinking of the bulky polymer and its enhanced stability in solvents. Meanwhile, the reaction between Li metal and proton-containing groups enhanced the interfacial contact during huge interface fluctuation. In this regard, a supramolecular copolymer based overlayer comprising of pendant poly(ethylene oxide) (PEO) segments and ureido-pyrimidinone (UPy) quadruple-hydrogen-bonding moieties was carefully investigated (Figure 4a).^[52] The PEO with abundant electronegative oxygen-containing segments provided strong binding with Li^+ . Moreover, the quadruple-hydrogen-bonding moieties in the UPy formed electrostatic chelation toward Li^+ , further enhancing the Li^+ -affinity. Benefited from this synergistic interaction with Li^+ , the resulting PEO-UPy overlayer provided ion-conductive networks with an ionic conductivity of 2.37×10^{-5} S/cm, indicating a fast Li^+ permeation and high rate performance. And the resulting Li metal anode had achieved stable cycling for 1000 h at a high areal capacity of 10 mAh/cm² and a high current density of 5 mA/cm². Despite of the above advantages, the reaction between Li and functional groups also caused extra consumption of active Li, which should be considered and minimized when constructing polar protective overlayers.^[16]

Beyond the strong interaction between Li^+ and functional groups, an electrokinetic phenomena of polar protective overlayer can further enhance Li^+ transport.^[53] The electrokinetic phenomenon is a tangential motion of liquid along a charged surface. In a protective overlayer with strong Li^+ -affinity, the electronegative surface adsorbed Li^+ to generate an electric double layer (EDL). When applied with electric field, the EDL-

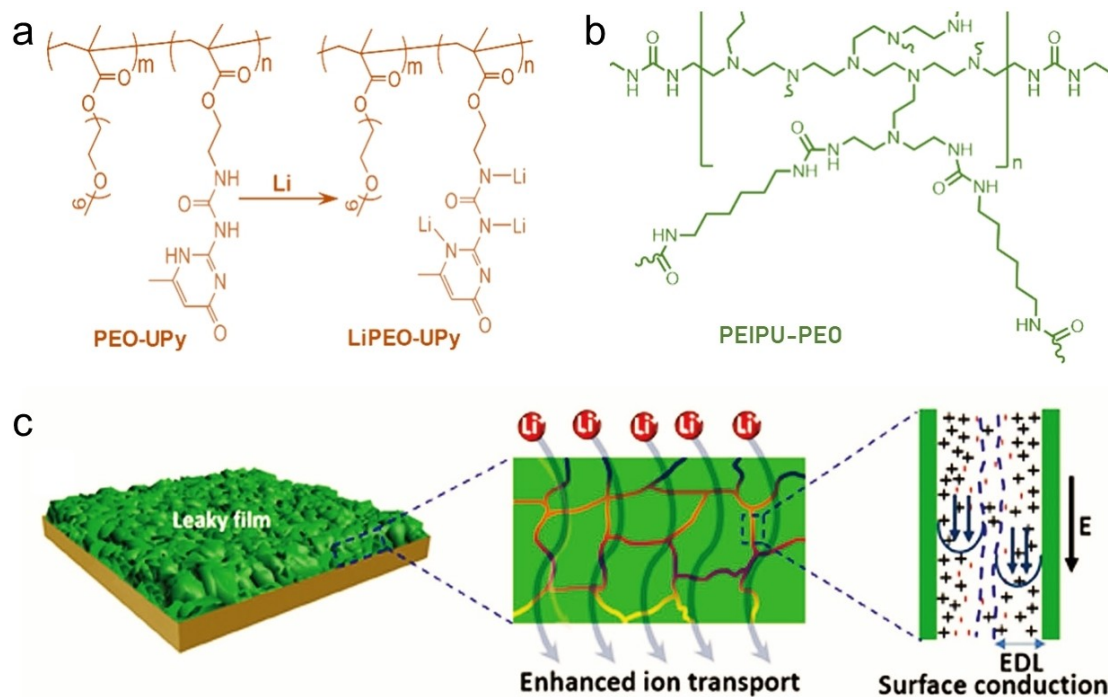


Figure 4. a) Chemical structure of the PEO-UPy protective overlayer and its binding with Li⁺. Reproduced with permission.^[52] Copyright 2019, Wiley-VCH. b) Chemical structure of the PEIPU-PEO protective overlayer. c) The electrokinetic surface conduction phenomena of the PEIPU-PEO protective overlayer to enhance Li⁺ transportation. Reproduced with permission.^[53] Copyright 2019, Wiley-VCH.

induced electrokinetic phenomena, for example, electrophoresis, electroosmosis, and surface conduction, contributed to largely enhanced Li⁺ transportation. As a typical paradigm, a super Li⁺-affinity overlayer was fabricated with cross-linked polyethylenimine (PEI)-based polyurea (PEIPU) and poly(ethylene oxide) (PEO) (Figure 4b). The Li⁺-affinity functional groups (e.g., –CO–NH–) drove the formation of the EDL, which pumped Li⁺ toward anode and concentrated Li⁺ at the anode vicinity.^[54] Consequently, Li⁺ depletion and ion concentration polarization were relieved that benefited a dendrite-free Li deposition (Figure 4c). The resulting Li metal anodes exhibited an outstanding rate performance of stable cycling at a high current density of 40 mA/cm² and a deposition capacity of 6 mAh/cm².

3.2. Non-polar polymers

The non-polar polymeric overlayers present weak interaction with Li⁺ and thus have poor Li⁺ conducting ability. Generally, the Li⁺ conducting behaviour of the non-polar polymeric overlayers derives from constructing porous structure in overlayers that allows electrolyte absorption to form Li⁺ transportation pathway. For instance, flexible polydimethylsiloxane (PDMS) with mechanical and chemical stability was employed as protective overlayer for Li metal after intentionally creating nanopores by acid treatment.^[46] The Li plating/stripping behaviour was highly relevant to the pore size of PDMS overlayer. Pore sizes around 40–400 nm were favourable to support Li⁺

transport and restrain dendrite penetration. Larger pores led to Li dendrite growth through the pores, and too small pores would retard the formation of ion conducting pathway and block Li⁺ transportation to anode surface. With this PDMS overlayer, Li metal anodes stably cycled for 800 h at 1 mA/cm² and 1 mAh/cm². Although non-polar polymeric overlayers help suppressing dendrite growth during cycling, their low Li⁺ conductivity and consequently poor rate performance of the Li metal anodes have limited their applications.

The swelling behaviour of polymeric protective overlayers is also a key parameter to be considered for the construction of Li metal anodes.^[45] As is known, polymeric structures with high swelling ratio generally possess more ionic channels inside. This will contribute to both increased ionic conductivity and rate capability of the resulting Li metal anodes. It should be also noted that, swelling may lead to dynamically structural change after the assembly of batteries, causing instability in the protective overlayer and nonuniform Li deposition. Therefore, it is important to seek a balance and leverage the swelling feature well for Li metal anodes. In this regard, combining polymeric structures with other non-swelling components or increasing the cross-linking degree are helpful to make the swelling behaviour controllable and tunable for optimized battery performances.

3.3. Polymeric-inorganic composites

Combining the flexibility of polymer with the strong mechanical strength of inorganic materials produces protective overlayers with improved structural integrity. Based on this concept, an organic/inorganic protective overlayer was explored with both enhanced mechanical strength and Li^+ conducting ability by mixing lithiated Nafion and LiCl salt.^[55] The lithiated Nafion polymer with Li^+ conducting $-\text{SO}_3\text{Li}$ groups provided a high ionic conductivity of $1.097 \times 10^{-4} \text{ S/cm}$, supporting fast Li^+ diffusion and homogeneous Li^+ flux. The LiCl salt endowed an enhanced Young's modulus of 6.12 GPa (higher than original solid-electrolyte interphase of 0.15 GPa) for the composite film, suggesting a dendrite blocking ability and more stable structure upon intensive volume change. With this hybrid protective overlayer, the Li metal anode achieved a cycle life over 400 cycles at 8 mA/cm^2 and 1 mAh/cm^2 . Designing rationally structured composite overlayer presents another promising strategy for Li^+ regulation, because it may produce unique Li^+ conducting behaviours.^[16,56,57] As a paradigm, a dual-layered protective overlayer was designed to include robust inner layer of rigid garnet Al-doped $\text{Li}_{6.75}\text{La}_3\text{Zr}_{1.75}\text{Ta}_{0.25}\text{O}_{12}$ (LLZTO) and flexible outer layer of lithiated Nafion (Figure 5a, b).^[58] The dual-layered structure rendered a single-ion conducting behaviour in the composite film, which was beneficial for fast Li^+ transportation and dendrite-free deposition. The Nafion top layer could extract Li^+ from the solvent sheath and then inject Li^+ into the LLZTO bottom layer, affording the single Li^+ conducting behaviour. As a result, the hybrid protective overlayer showed an ionic conductivity of $3 \times 10^{-5} \text{ S/cm}$, a drastically

improved t_{Li^+} of 0.82, and a compressed Li^+ concentration gradient at the anode vicinity (Figure 5c, d).

4. Carbonaceous Materials

Carbonaceous materials with excellent chemical stability, strong mechanical strength, light weight, and tunable nanostructure, are regarded as excellent choices for protective overlayers of Li metal anodes.^[59,60] Their strong mechanical strength, for example, over 200 GPa, enables the resulting overlayers to effectively block dendrite penetration.^[61] Meanwhile, the carbonaceous protective overlayer are also able to alter the distribution and transportation of Li^+ through their unique electronegative π -electrons that presents strong interaction with Li^+ .^[62]

Carbonaceous materials present a Fermi level at $\sim 5.0 \text{ eV}$, in contrast to $\sim 2.9 \text{ eV}$ of Li metal.^[63,64] This difference in Fermi level yields an electrochemical potential between two materials (also known as Volta or contact potential), enabling a spontaneous reduction and lithiation of carbonaceous materials by Li metal. The lithiated carbonaceous materials play a special role in regulating Li^+ transportation. As a typical example, a lithiated multiwalled carbon nanotube (Li-MWCNT) protective overlayer was employed to improve Li^+ transportation.^[65] The Li-MWCNT overlayer was in situ constructed through the physical contact between an electrolyte-wetted MWCNT film and a Li metal foil (Figure 6a). Then the contact potential drove a spontaneous reduction and lithiation of MWCNT. The Li-MWCNT overlayer served as a Li^+ reservoir and a Li^+ diffusion mediator, which guided uniform Li deposition underneath the overlayer. The Li^+ stored in the Li-MWCNT was first plated on Li metal surface and

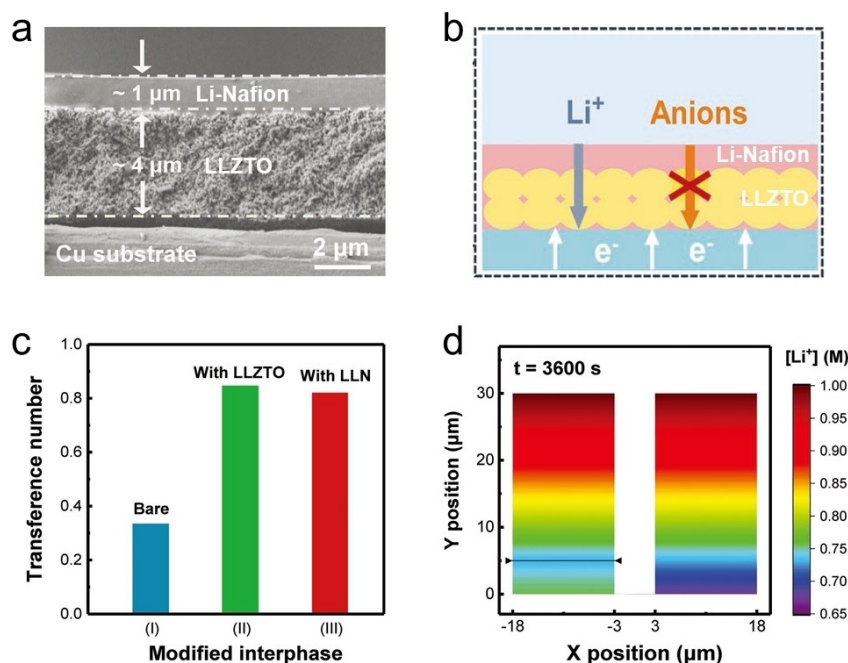


Figure 5. a) The cross-sectional SEM image of the dual-layered protective overlayer. b) Schematic of the dual-layered protective overlayer and its single-ion-conducting behaviour. c) The Li^+ transference numbers for different overlayers. d) The finite element method simulation results of Li^+ concentration distribution upon Li plating with (left) and without (right) protective overlayer. Reproduced with permission.^[58] Copyright 2019, Wiley-VCH.

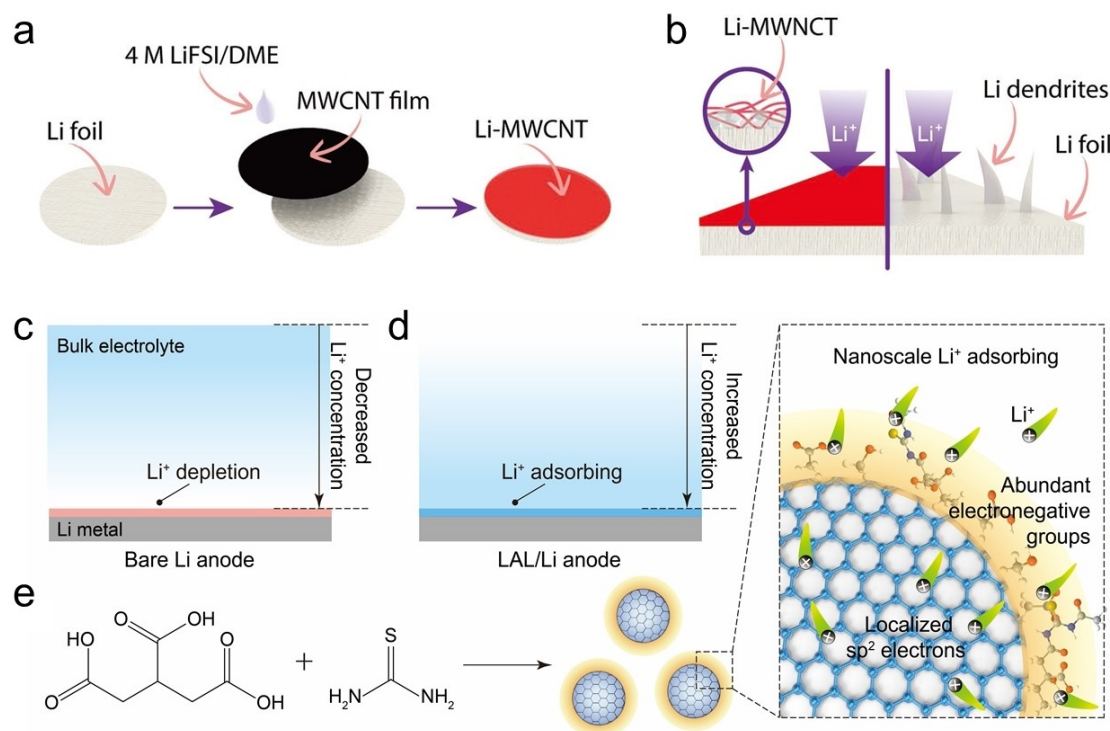


Figure 6. a) Schematic of the fabrication process of the Li-MWCNT protected Li metal anode. b) Schematic of the dendrite-free Li deposition with Li-MWCNT protective overlayer. Reproduced with permission.^[65] Copyright 2018, Wiley-VCH. c) and d) Schematics of the Li^+ depletion without LAL and Li^+ adsorbing with LAL protective overlayer upon Li deposition, respectively. e) Schematic of the preparation process and design rationale of the graphene quantum dot building blocks for the LAL. Reproduced with permission.^[68] Copyright 2021, Wiley-VCH.

then refilled from electrolyte during Li plating, and a reversed process was conducted upon Li stripping (Figure 6b). The resulting Li metal anode achieved a long cycle life for 1000 h at 2 mA/cm^2 and 4 mAh/cm^2 . This strategy of altering the Li^+ diffusion pathway presented a promising method to homogenize Li^+ distribution and reduce Li^+ concentration polarization for high-performance Li metal anodes. Particularly, the employment of aromatic carbon as intermediate layer was beneficial, because it selectively intercalated Li^+ and prevented the intercalation of larger anions (e.g., PF_6^- , FSI^- , and TFSI^-).^[66,67]

Reducing the size of carbonaceous building blocks for protective overlayers demonstrates an effective strategy to enhance the Li^+ diffusion and homogenize Li^+ distribution. In this regard, we synthesized zero-dimensional quantum-sized graphene dots and then constructed an ultrathin Li^+ adsorbing layer (LAL) on Li metal surface (Figure 6c, d).^[68] The graphene quantum dots exhibited typical sizes of 3–5 nm, and they were comprised of nanocrystalline carbon cores with surface polar functional groups (e.g., $-\text{OH}$, $-\text{NH}_2$, $\text{C}=\text{O}/\text{C}=\text{N}$, and $\text{C}=\text{S}$). This unique quantum-sized graphene dots could localize the sp^2 -electrons that induced attraction forces toward Li^+ . Moreover, they presented large amount of edge sites that afforded enhanced surface grafting of electronegative functional groups to achieve superior Li^+ -affinity (Figure 6e). According to the DFT simulations, the graphene quantum dot exhibited strong interaction with Li^+ at the molecular level due to its increased localized negative charges. This strong interaction was advanta-

geous to adsorb and concentrate Li^+ at the Li metal surface in a uniform manner which resulted in a relieved Li^+ depletion, a uniform Li^+ flux (Figure 6d). Meanwhile, Li^+ could penetrate through the LAL and deposit beneath the LAL, leading to the continuous Li^+ adsorbing effect and dendrite-free Li deposition. With the protection of LAL, the Li metal anode exhibited an excellent rate performance upon a spectrum of current densities from 1 to 60 mA/cm^2 with only marginally increased overpotentials. And the LAL/Li anode even stably cycled for over 1000 h at both ultrahigh current density of 60 mA/cm^2 and areal capacity of 60 mAh/cm^2 . By designing the molecular structure and synthetic route, various carbon quantum dots with outstanding properties can be obtained and may further enhance the electrochemical performances of Li metal anodes.^[69,70] It should be noted that carbonaceous materials with relatively high electronic conductivities may cause Li deposition in or above the resulting overlayers, invalidating the functionality of protective overlayers.^[59] Reducing the electrical conductivities of carbonaceous materials can relieve this problem to some extent.^[71,72]

5. Others

Porous materials with subnanochannels, such as covalent organic frameworks (COFs) and metal-organic frameworks (MOFs), are drawing attention for constructing artificial protec-

tive overlayers due to their extraordinary characteristics, including tunable porosity, structural diversity, and strong mechanical strength.^[73,74] Their unique narrow subnanochannels can be elaborately tuned to allow Li^+ transportation and block the bulky anions or solvents. This selected Li^+ transportation is beneficial for improving the Li^+ transfer efficiency and facilitating fast Li^+ replenishment to inhibit Li^+ depletion. The large specific surface area of MOFs and COFs is also advantageous to homogenize Li^+ flux and induce smooth Li depositing.

Under this guideline, a protective overlayer was prepared by employing 2D anionic covalent frameworks on Li metal surface for dendrite suppression (Figure 7a).^[75] These 2D nanosheets possessed a hexagonal honeycomb-like network with nanoporosity (Figure 7b). The comparable size between the nanopore channel (~ 0.6 nm) and the PF_6^- anion (~ 0.5 nm) caused steric confinement that hindered penetration of anion, while facilitated the Li^+ transportation (Figure 7b). This phenomenon enabled a higher Li^+ mobility over anion and consequently a near-unity t_{Li^+} of 0.82. Moreover, the layered anionic frameworks shortened the translocation distance of Li^+ and provided a superior ionic conductivity ($> 10^{-3}$ S/cm). The synergy of both high t_{Li^+} and ionic conductivity was conducive to eliminating Li^+ depletion in the anode vicinity and promoting dendrite-free deposition. The function mode of porous organic frameworks had been further clarified from the viewpoint of thermodynamics.^[76] The MOFs could selectively exclude extra solvent molecules within a Li^+ solvation sheath and reduce the desolvation energy barrier of Li^+ , leading to an easier access of Li^+ to Li metal anode and a facilitated Li deposition process (Figure 7c, d). With the MOF overlayer, the Li metal anode exhibited a plating/stripping overpotential at

merely 100 mV at a current density of 3 mA/cm^2 , verifying the effectively reduced energy barrier and facilitated Li^+ transportation. Except for COFs and MOFs, other types of porous materials, such as hydrogen-bonded organic frameworks, polyoxometalates, and porous organic crystals, also show great potential to promote Li^+ transportation and achieve stable Li metal anodes.^[77]

6. Conclusions and Perspectives

In summary, artificial protective overlayers with designed components and structures are effective to enable dendrite-free and high-performance Li metal anodes for next-generation high-energy-density batteries. In this Concept article, we have highlighted the recent advance of artificial protective overlayers under the category of inorganic, polymeric, and carbonaceous overlayers with an emphasis on their influence on interfacial Li^+ distribution. We conclude this work with some perspectives on the remaining challenges and future directions as follows:

Mechanism understanding and model constructing. The establishment of an accurate mathematical correlation between ionic conductivity or mechanical properties of protective overlayers and Li dendrite inhibition is important to better understand how the protective overlayers can be optimized. For instance, modeling and quantifying the effect of ionic conductivity/mechanical strength on the Li depositing morphology, can yield an optimum parameter for dendrite suppression and guide the material screening process. In addition, based on the experimental and theoretical results, a material database of protective overlayer should be established and the artificial

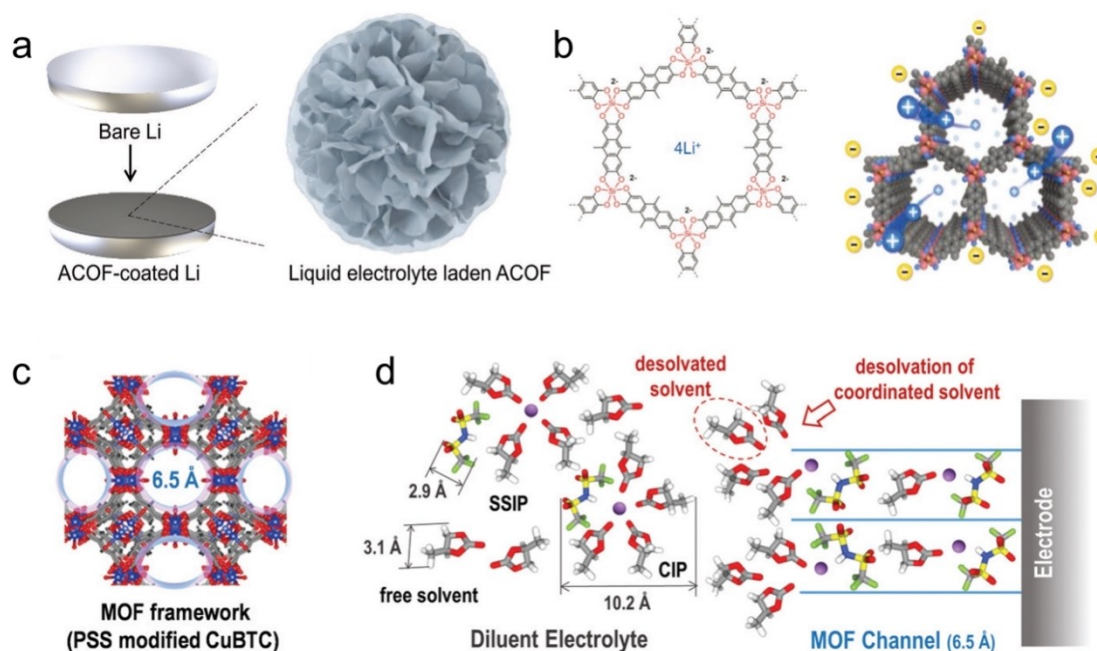


Figure 7. a) Schematic of the ACOF-coated Li metal anode and the ACOF constructed by particles of 2D nanosheets. b) The chemical structure of the ACOF and the selective ion transport in ACOF. Reproduced with permission.^[75] Copyright 2020, Wiley-VCH. c) and d) Schematics of the sub-nanostructure in the MOF protective overlayer and the electrolyte structure inside MOF channels, respectively. Reproduced with permission.^[76] Copyright 2021, Wiley-VCH.

intelligence of machine learning can be further utilized to predict and guide the design of protective overlayers.

Electrochemical performances. Despite of achievements in extending cycle life of Li metal anodes by artificial protective overlayers, the cycling current density and areal capacity are still far from the high-power outputs and fast charging of advanced battery systems. In this regard, the protective overlayer should possess high ionic conductivity to allow rapid Li⁺ permeation that prevents Li⁺ depletion at electrode surface upon high-rate cycling. Simultaneously, the protective overlayer should be strong and flexible enough to withstand the large volume change upon high-areal-capacity cycling. As single material can hardly meet all the requirements, rationally designed composite protective overlayers present a promising solution.

Scalable production. The highly reactive nature of Li metal toward oxygen and moisture in ambient air has confined the fabrication of Li metal-based battery in argon-filled glove box, which hinders their large-scale manufacturing and increases production costs. Artificial protective overlayers possess unique advantages in promoting the air-stability of Li metal anode. In consideration of water-proof ability, protective overlayers with large water contact angle are favourable. But the hydrophobicity may cause poor Li⁺ conductivity and undermined electrochemical performances. Thus, a tradeoff between water-proof ability and Li⁺ conductivity is required. Blocking oxygen is more difficult than water and the so far reported Li metal anodes exhibit unsatisfying air endurance within only several hours. Breakthroughs in component and structure of protective overlayers are required to address these problems. In addition, the construction method of protective overlayers should be carefully valued upon industrial application. The chemical vapor deposition method allows a precise control in thickness and uniformity of the overlayer, but this method is complex, time-consuming and expensive. In comparison, solution casting methods like dip-coating, spin-coating, and spray-casting are low-cost and scalable, exhibiting greater potentials in large-scale manufacturing.

The uniform Li⁺ distribution and fast Li⁺ transportation at electrode surface are essential for dendrite-free and high-performance Li metal anodes, while remain challenging and need further investigation. We believe that with the development of material science and manufacturing technology, breakthroughs in artificial protective overlayers are foreseeable and the Li metal anodes will achieve fast charge and high-capacity goals with long life span. We hope this progress report provides valuable information and insights for the future research on artificial protective overlayers for high-performance Li metal batteries.

Acknowledgements

This work was supported by MOST (2016YFA0203302), NSFC (21634003), STCSM (20JC1414902, 18QA1400700), SHMEC (201-01-07-00-07-E00062).

Conflict of Interest

The authors declare no conflict of interest.

Data Availability Statement

The data that support the findings of this study are available from the corresponding author upon reasonable request.

Keywords: artificial protective overlayer · batteries · ion distribution · ion transportation · lithium metal

- [1] Y. Li, Y. Li, A. Pei, K. Yan, Y. Sun, C. L. Wu, L. M. Joubert, R. Chin, A. L. Koh, Y. Yu, J. Perrino, B. Butz, S. Chu, Y. Cui, *Science* **2017**, *358*, 506.
- [2] J. Liu, Z. Bao, Y. Cui, E. J. Dufek, J. B. Goodenough, P. Khalifah, Q. Li, B. Y. Liaw, P. Liu, A. Manthiram, Y. S. Meng, V. R. Subramanian, M. F. Toney, V. V. Viswanathan, M. S. Whittingham, J. Xiao, W. Xu, J. Yang, X. Q. Yang, J. G. Zhang, *Nat. Energy* **2019**, *4*, 180–186.
- [3] D. H. Liu, Z. Bai, M. Li, A. Yu, D. Luo, W. Liu, L. Yang, J. Lu, K. Amine, Z. Chen, *Chem. Soc. Rev.* **2020**, *49*, 5407–5445.
- [4] Y. Zhang, T. T. Zuo, J. Popovic, K. Lim, Y. X. Yin, J. Maier, Y. G. Guo, *Mater. Today* **2020**, *33*, 56–74.
- [5] Z. Wang, Z. Sun, J. Li, Y. Shi, C. Sun, B. An, H. M. Cheng, F. Li, *Chem. Soc. Rev.* **2021**, *50*, 3178–3210.
- [6] P. Zou, Y. Sui, H. Zhan, C. Wang, H. L. Xin, H. M. Cheng, F. Kang, C. Yang, *Chem. Rev.* **2021**, *121*, 5986–6056.
- [7] J. N. Chazalviel, *Phys. Rev. A* **1990**, *42*, 7355–7367.
- [8] X. Xu, Y. Liu, J. Y. Hwang, O. O. Kapitanova, Z. Song, Y. K. Sun, A. Matic, S. Xiong, *Adv. Energy Mater.* **2020**, *10*, 2002390.
- [9] J. Pu, J. Li, K. Zhang, T. Zhang, C. Li, H. Ma, J. Zhu, P. V. Braun, J. Lu, H. Zhang, *Nat. Commun.* **2019**, *10*, 1896.
- [10] L. Ye, M. Liao, H. Sun, Y. Yang, C. Tang, Y. Zhao, L. Wang, Y. Xu, L. Zhang, B. Wang, F. Xu, X. Sun, Y. Zhang, H. Dai, P. G. Bruce, H. Peng, *Angew. Chem. Int. Ed.* **2019**, *58*, 2437–2442; *Angew. Chem.* **2019**, *131*, 2459–2464.
- [11] Z. Sun, S. Jin, H. Jin, Z. Du, Y. Zhu, A. Cao, H. Ji, L. J. Wan, *Adv. Mater.* **2018**, *30*, 1800884.
- [12] H. Chen, Y. Yang, D. T. Boyle, Y. K. Jeong, R. Xu, L. S. de Vasconcelos, Z. Huang, H. Wang, H. Wang, W. Huang, H. Li, J. Wang, H. Gu, R. Matsumoto, K. Motohashi, Y. Nakayama, K. Zhao, Y. Cui, *Nat. Energy* **2021**, *6*, 790–798.
- [13] L. Fan, S. Li, L. Liu, W. Zhang, L. Gao, Y. Fu, F. Chen, J. Li, H. L. Zhuang, Y. Lu, *Adv. Energy Mater.* **2018**, *8*, 1802350.
- [14] J. Fu, X. Ji, J. Chen, L. Chen, X. Fan, D. Mu, C. Wang, *Angew. Chem. Int. Ed.* **2020**, *59*, 22194–22201; *Angew. Chem.* **2020**, *132*, 22378–22385.
- [15] N. von Aspern, G. V. Röschenthaler, M. Winter, I. Laskovic, *Angew. Chem. Int. Ed.* **2019**, *58*, 15978–16000; *Angew. Chem.* **2019**, *131*, 16124–16147.
- [16] Y. Gao, Z. Yan, J. L. Gray, X. He, D. Wang, T. Chen, Q. Huang, Y. C. Li, H. Wang, S. H. Kim, T. E. Mallouk, D. Wang, *Nat. Mater.* **2019**, *18*, 384–389.
- [17] R. Xu, X. B. Cheng, C. Yan, X. Q. Zhang, Y. Xiao, C. Z. Zhao, J. Q. Huang, Q. Zhang, *Matter* **2019**, *1*, 317–344.
- [18] M. S. Kim, J. H. Ryu, Deepika, Y. R. Lim, I. W. Nah, K. R. Lee, L. A. Archer, W. Cho, *Nat. Energy* **2018**, *3*, 889–898.
- [19] N. W. Li, Y. X. Yin, C. P. Yang, Y. G. Guo, *Adv. Mater.* **2016**, *28*, 1853–1858.
- [20] W. Chen, R. V. Salvatierra, M. Ren, J. Chen, M. G. Stanford, J. M. Tour, *Adv. Mater.* **2020**, *32*, 2002850.
- [21] D. Zhang, S. Wang, B. Li, Y. Gong, S. Yang, *Adv. Mater.* **2019**, *31*, 1901820.
- [22] Y. Zhou, X. Zhang, Y. Ding, J. Bae, X. Guo, Y. Zhao, G. Yu, *Adv. Mater.* **2020**, *32*, 2003920.
- [23] M. L. Meyerson, P. E. Papa, A. Heller, C. B. Mullins, *ACS Nano* **2021**, *15*, 29–46.
- [24] M. D. Tikekar, S. Choudhury, Z. Tu, L. A. Archer, *Nat. Energy* **2016**, *1*, 16114.
- [25] G. Li, *Adv. Energy Mater.* **2021**, *11*, 2002891.
- [26] K. Zhang, W. Liu, Y. Gao, X. Wang, Z. Chen, R. Ning, W. Yu, R. Li, L. Li, X. Li, K. Yuan, L. Ma, N. Li, C. Shen, W. Huang, K. Xie, K. P. Loh, *Adv. Mater.* **2021**, *33*, 2006323.
- [27] D. Kang, M. Xiao, J. P. Lemmon, *Batteries & Supercaps* **2021**, *4*, 445–455.

- [28] J. Zhu, P. Li, X. Chen, D. Legut, Y. Fan, R. Zhang, Y. Lu, X. Cheng, Q. Zhang, *Energy Storage Mater.* **2019**, *16*, 426–433.
- [29] Y. Li, Y. Sun, A. Pei, K. Chen, A. Vailionis, Y. Li, G. Zheng, J. Sun, Y. Cui, *ACS Cent. Sci.* **2018**, *4*, 97–104.
- [30] M. Baloch, D. Shanmukaraj, O. Bondarchuk, E. Bekaert, T. Rojo, M. Armand, *Energy Storage Mater.* **2017**, *9*, 141–149.
- [31] K. Park, J. B. Goodenough, *Adv. Energy Mater.* **2017**, *7*, 1700732.
- [32] K. Chen, R. Pathak, A. Gurung, E. A. Adhamash, B. Bahrami, Q. He, H. Qiao, A. L. Smirnova, J. J. Wu, Q. Qiao, Y. Zhou, *Energy Storage Mater.* **2019**, *18*, 389–396.
- [33] L. Suo, W. Xue, M. Gobet, S. G. Greenbaum, C. Wang, Y. Chen, W. Yang, Y. Li, J. Li, *Proc. Natl. Acad. Sci. USA* **2018**, *115*, 1156.
- [34] T. Li, X. Q. Zhang, P. Shi, Q. Zhang, *Joule* **2019**, *3*, 2647–2661.
- [35] A. Wang, S. Kadam, H. Li, S. Shi, Y. Qi, *npj Comput. Mater.* **2018**, *4*, 15.
- [36] H. Yildirim, A. Kinaci, M. K. Y. Chan, J. P. Greeley, *ACS Appl. Mater. Interfaces* **2015**, *7*, 18985–18996.
- [37] Z. Peng, N. Zhao, Z. Zhang, H. Wan, H. Lin, M. Liu, C. Shen, H. He, X. Guo, J. G. Zhang, D. Wang, *Nano Energy* **2017**, *39*, 662–672.
- [38] L. Fan, H. L. Zhuang, L. Gao, Y. Lu, L. A. Archer, *J. Mater. Chem. A* **2017**, *5*, 3483–3492.
- [39] X. Liang, Q. Pang, I. R. Kochetkov, M. S. Sempere, H. Huang, X. Sun, L. F. Nazar, *Nat. Energy* **2017**, *2*, 17119.
- [40] Z. Lu, W. Li, Y. Long, J. Liang, Q. Liang, S. Wu, Y. Tao, Z. Weng, W. Lv, Q. H. Yang, *Adv. Funct. Mater.* **2020**, *30*, 1907343.
- [41] Y. Zhang, G. Wang, L. Tang, J. Wu, B. Guo, M. Zhu, C. Wu, S. X. Dou, M. Wu, *J. Mater. Chem. A* **2019**, *7*, 25369–25376.
- [42] W. Liu, P. Liu, D. Mitlin, *Adv. Energy Mater.* **2020**, *10*, 2002297.
- [43] N. W. Li, Y. Shi, Y. X. Yin, X. X. Zeng, J. Y. Li, C. J. Li, L. J. Wan, R. Wen, Y. G. Guo, *Angew. Chem. Int. Ed.* **2018**, *57*, 1505–1509; *Angew. Chem.* **2018**, *130*, 1521–1525.
- [44] J. Lopez, A. Pei, J. Y. Oh, G. Wang, Y. Cui, Z. Bao, *J. Am. Chem. Soc.* **2018**, *140*, 11735–11744.
- [45] J. Li, Y. Cai, H. Wu, Z. Yu, X. Yan, Q. Zhang, T. Z. Gao, K. Liu, X. Jia, Z. Bao, *Adv. Energy Mater.* **2021**, *11*, 2003239.
- [46] B. Zhu, Y. Jin, X. Hu, Q. Zheng, S. Zhang, Q. Wang, J. Zhu, *Adv. Mater.* **2017**, *29*, 1603755.
- [47] Y. Sun, Y. Zhao, J. Wang, J. Liang, C. Wang, Q. Sun, X. Lin, K. R. Adair, J. Luo, D. Wang, R. Li, M. Cai, T. K. Sham, X. Sun, *Adv. Mater.* **2019**, *31*, 1806541.
- [48] F. Shen, K. Wang, Y. Yin, L. Shi, D. Zeng, X. Han, *J. Mater. Chem. A* **2020**, *8*, 6183–6189.
- [49] Y. Hong, X. Cheng, G. Liu, D. Hong, S. He, B. Wang, X. Sun, H. Peng, *Chin. J. Polym. Sci.* **2019**, *37*, 737–743.
- [50] J. Luo, C. C. Fang, N. L. Wu, *Adv. Energy Mater.* **2018**, *8*, 1701482.
- [51] P. Martins, A. C. Lopes, S. Lanceros-Mendez, *Prog. Polym. Sci.* **2014**, *39*, 683–706.
- [52] G. Wang, C. Chen, Y. Chen, X. Kang, C. Yang, F. Wang, Y. Liu, X. Xiong, *Angew. Chem. Int. Ed.* **2020**, *59*, 2055–2060; *Angew. Chem.* **2020**, *132*, 2071–2076.
- [53] G. Li, Z. Liu, D. Wang, X. He, S. Liu, Y. Gao, A. Zahrani, S. H. Kim, L. Q. Chen, D. Wang, *Adv. Energy Mater.* **2019**, *9*, 1900704.
- [54] G. Li, Z. Liu, Q. Huang, Y. Gao, M. Regula, D. Wang, L. Q. Chen, D. Wang, *Nat. Energy* **2018**, *3*, 1076–1083.
- [55] S. Li, L. Fan, Y. Lu, *Energy Storage Mater.* **2019**, *18*, 205–212.
- [56] Q. Pang, L. Zhou, L. F. Nazar, *Proc. Natl. Acad. Sci. USA* **2018**, *115*, 12389.
- [57] Y. Gu, W. W. Wang, Y. J. Li, Q. H. Wu, S. Tang, J. W. Yan, M. S. Zheng, D. Y. Wu, C. H. Fan, W. Q. Hu, Z. B. Chen, Y. Fang, Q. H. Zhang, Q. F. Dong, B. W. Mao, *Nat. Commun.* **2018**, *9*, 1339.
- [58] R. Xu, Y. Xiao, R. Zhang, X. B. Cheng, C. Z. Zhao, X. Q. Zhang, C. Yan, Q. Zhang, J. Q. Huang, *Adv. Mater.* **2019**, *31*, 1808392.
- [59] D. Lin, Y. Liu, Y. Cui, *Nat. Nanotechnol.* **2017**, *12*, 194–206.
- [60] H. Ye, S. Xin, Y. X. Yin, Y. G. Guo, *Adv. Energy Mater.* **2017**, *7*, 1700530.
- [61] Y. Liu, Y. K. Tzeng, D. Lin, A. Pei, H. Lu, N. A. Melosh, Z. X. Shen, S. Chu, Y. Cui, *Joule* **2018**, *2*, 1595–1609.
- [62] H. Ye, S. Xin, Y. X. Yin, J. Y. Li, Y. G. Guo, L. J. Wan, *J. Am. Chem. Soc.* **2017**, *139*, 5916–5922.
- [63] S. Halas, T. Durakiewicz, *J. Phys. Condens. Matter* **1998**, *10*, 10815–10826.
- [64] Y. Liu, H. Zheng, X. H. Liu, S. Huang, T. Zhu, J. Wang, A. Kushima, N. S. Hudak, X. Huang, S. Zhang, S. X. Mao, X. Qian, J. Li, J. Y. Huang, *ACS Nano* **2011**, *5*, 7245–7253.
- [65] R. V. Salvatierra, G. A. López-Silva, A. S. Jalilov, J. Yoon, G. Wu, A. L. Tsai, J. M. Tour, *Adv. Mater.* **2018**, *30*, 1803869.
- [66] Y. Liu, Y. Cui, *Joule* **2017**, *1*, 649–650.
- [67] C. Uhlmann, J. Illig, M. Ender, R. Schuster, E. Tiffée, *J. Power Sources* **2015**, *279*, 428–438.
- [68] L. Ye, M. Liao, X. Cheng, X. Zhou, Y. Zhao, Y. Yang, C. Tang, H. Sun, Y. Gao, B. Wang, H. Peng, *Angew. Chem. Int. Ed.* **2021**, *60*, 17419–17425.
- [69] S. Zhu, Y. Song, J. Shao, X. Zhao, B. Yang, *Angew. Chem. Int. Ed.* **2015**, *54*, 14626–14637; *Angew. Chem.* **2015**, *127*, 14834–14846.
- [70] Q. Liu, J. Sun, K. Gao, N. Chen, X. Sun, D. Ti, C. Bai, R. Cui, L. Qu, *Mater. Chem. Front.* **2020**, *4*, 421–436.
- [71] G. Zheng, S. W. Lee, Z. Liang, H. W. Lee, K. Yan, H. Yao, H. Wang, W. Li, S. Chu, Y. Cui, *Nat. Nanotechnol.* **2014**, *9*, 618–623.
- [72] W. Guo, S. Liu, X. Guan, X. Zhang, X. Liu, J. Luo, *Adv. Energy Mater.* **2019**, *9*, 1900193.
- [73] C. Li, L. Liu, J. Kang, Y. Xiao, Y. Feng, F. F. Cao, H. Zhang, *Energy Storage Mater.* **2020**, *31*, 115–134.
- [74] Y. He, Y. Qiao, Z. Chang, H. Zhou, *Energy Environ. Sci.* **2019**, *12*, 2327–2344.
- [75] X. Li, Y. Tian, L. Shen, Z. Qu, T. Ma, F. Sun, X. Liu, C. Zhang, J. Shen, X. Li, L. Gao, S. Xiao, T. Liu, Y. Liu, Y. Lu, *Adv. Funct. Mater.* **2021**, *31*, 2009718.
- [76] Z. Chang, Y. Qiao, H. Yang, H. Deng, X. Zhu, P. He, H. Zhou, *Energy Environ. Sci.* **2020**, *13*, 4122–4131.
- [77] S. Chand, S. M. Elahi, A. Pal, M. C. Das, *Chem. Eur. J.* **2019**, *25*, 6259–6269.

Manuscript received: September 11, 2021
Accepted manuscript online: November 2, 2021
Version of record online: February 1, 2022